Improved assessment of gross and net primary productivity of Canada's landmass

Alemu Gonsamo,[1] Jing M. Chen,[1] David T. Price,[2] Werner A. Kurz,[3] Jane Liu,[1] Céline Boisvenue,[3] Robbie A. Hember,[3,4] Chaoyang Wu,[1] and Kuo-Hsien Chang[1]

Received 21 May 2013; revised 3 October 2013; accepted 14 October 2013; published 25 November 2013.

[1] We assess Canada's gross primary productivity (GPP) and net primary productivity (NPP) using boreal ecosystem productivity simulator (BEPS) at 250 m spatial resolution with improved input parameter and driver fields and phenology and nutrient release parameterization schemes. BEPS is a process-based two-leaf enzyme kinetic terrestrial ecosystem model designed to simulate energy, water, and carbon (C) fluxes using spatial data sets of meteorology, remotely sensed land surface variables, soil properties, and photosynthesis and respiration rate parameters. Two improved key land surface variables, leaf area index (LAI) and land cover type, are derived at 250 m from Moderate Resolution Imaging Spectroradiometer sensor. For diagnostic error assessment, we use nine forest flux tower sites where all measured C flux, meteorology, and ancillary data sets are available. The errors due to input drivers and parameters are then independently corrected for Canada-wide GPP and NPP simulations. The optimized LAI use, for example, reduced the absolute bias in GPP from 20.7% to 1.1% for hourly BEPS simulations. Following the error diagnostics and corrections, daily GPP and NPP are simulated over Canada at 250 m spatial resolution, the highest resolution simulation yet for the country or any other comparable region. Total NPP (GPP) for Canada's land area was 1.27 (2.68) Pg C for 2008, with forests contributing 1.02 (2.2) Pg C. The annual comparisons between measured and simulated GPP show that the mean differences are not statistically significant ($p > 0.05$, paired t test). The main BEPS simulation error sources are from the driver fields.

Citation: Gonsamo, A., J. M. Chen, D. T. Price, W. A. Kurz, J. Liu, C. Boisvenue, R. A. Hember, C. Wu, and K.-H. Chang (2013), Improved assessment of gross and net primary productivity of Canada's landmass, *J. Geophys. Res. Biogeosci.*, *118*, 1546–1560, doi:10.1002/2013JG002388.

1. Introduction

[2] Terrestrial ecosystem process models of varying complexity and structure have been developed over the years to gain insights into the processes that might explain changes in overall atmosphere–biosphere carbon (C) fluxes [e.g., *Sellers et al.*, 1986; *Running and Coughlan*, 1988; *Potter et al.*, 1993; *Liu et al.*, 1997; *Chen et al.*, 2000; *Ren et al.*, 2011; *Larjavaara and Muller-Landau*, 2012]. Process-based models integrate and formalize knowledge of ecological processes and allow observations at various scales to be incorporated into regional and global analyses [*Chen et al.*, 2012]. Such models typically require estimates of rate parameters and surface characteristics, along with a set of meteorological and vegetation driving variables, from which estimates of state vectors such as gross primary productivity (GPP) and net primary productivity (NPP) are simulated.

[3] Regional validation and analysis of ecosystem process models are complicated by the difficulty in measuring and setting parameters and reference state vectors and finding adequate data to drive the model. One method of validation is to compare model results with C flux measurements, the exchange of C between atmosphere and biosphere, obtained in different ecosystem types from global networks of fluxnet tower sites. With access to flux tower data, ecosystem process models can also be diagnostically evaluated for the relative contributions of parameter and driver uncertainties by incorporating as many measured parameter and driver fields as possible. It is through such comparisons that we can improve the models and gain better scientific understanding of the C cycle processes at the ecosystem scale.

[4] Although many ancillary data sets exist at global networks of C flux sites, previous studies have often focused on statistical optimization methods to constrain model uncertainty and possible errors from the driver and parameter fields [*Santaren et al.*, 2007; *Groenendijk et al.*, 2011].

Additional supporting information may be found in the online version of this article.

[1]Department of Geography and Program in Planning, University of Toronto, Toronto, Ontario, Canada.
[2]Northern Forestry Centre, Canadian Forest Service, Natural Resources Canada, Edmonton, Alberta, Canada.
[3]Pacific Forestry Centre, Canadian Forest Service, Natural Resources Canada, Victoria, British Columbia, Canada.
[4]Faculty of Forestry, University of British Columbia, Vancouver, British Columbia, Canada.

Corresponding author: A. Gonsamo, Department of Geography and Program in Planning, University of Toronto, Rm. 5047, Sidney Smith Hall, 100 St. George St., Toronto, Ontario M5S 3G3, Canada. (gonsamoa@geog.utoronto.ca)

2169-8953/13/10.1002/2013JG002388

[5] Model parameters (e.g., maximum carboxylation rate of Rubisco: V_m) may be impractical to measure over extensive regions, while driver fields (e.g., meteorology, and remotely sensed leaf area index (LAI) products) are rarely complete, with data gaps due to sensor failure, data contamination, and sparse observational networks. Driver fields may be interpolated from available data sources [e.g., *Jeffrey et al*., 2001; *Lafont et al*., 2012], while parameters are generally retrieved through inversion or optimization methods [e.g., *Santaren et al*., 2007; *Groenendijk et al*., 2011]. The downside of this strategy is the unavoidable interference of model errors during the data assimilation process through parameter and driver optimizations. Any optimization method for retrieval of key model parameters and drivers requires characterizing the measurement error, the model error (stemming from inappropriate equation forms or from missing processes in the C cycle model structure), the error brought by the driver data, and the parameter error distributions arising from inadequate knowledge about a series of parameters. Even within the basic assumption of normally distributed errors, this characterization involves potentially large error covariance matrices from different error terms. Optimization equations are often imposed to the inversion as a strong constraint, even though many ecosystem process models are run on coarse spatial grids involving several land cover types and plant functional types (PFTs). Multisite or large-scale high spatial resolution parameter optimization would require large computing resources and are not practical. The optimization process is often statistical and arbitrary because all interacting parameter and driver spaces cannot be optimized simultaneously in a way that can be extrapolated to larger area simulations. One possible solution would be the use of as many measured parameters and drivers as possible to compute the relative error sources and apply corrections independently. This however has not been practical so far because the parameters are generally defined for individual land cover types or PFTs which cannot be resolved in coarse resolution for regional or global simulations. In this study, we carry out GPP and NPP simulations using measured parameter and driver fields, at high spatial resolution (250 m) to tackle this problem.

[6] *Liu et al*. [2002] simulated NPP at 1 km spatial resolution using ecosystem process model over Canada for the first time, partially resolving parameter assignment problems in the mixed grid cells, those consisting of several land cover types. However, spatial Fourier analysis conducted over North America's agricultural regions showed two spectral satellite measurement maxima at the 200–300 m and 400–700 m length scales which characterize the typical size of various land cover types [*Trishchenko*, 2004]. Therefore, a 250 m spatial resolution appears highly suitable for gridded parameterization of ecosystem process models over Canada, because it will generally resolve the shorter of these two measurement maxima. The daily global remote sensing observations available at 250 m resolution provide opportunities to perform continental-scale simulations at unprecedentedly high spatial resolution setting.

[7] In this study, the boreal ecosystem productivity simulator (BEPS) is used to simulate GPP and NPP over Canada at daily [*Liu et al*., 2002] and hourly [*Ju et al*., 2006; *Chen et al*., 2007; *Chen et al*., 2012; *Sprintsin et al*., 2012] timescales. This study aims to examine and compare the magnitudes of BEPS errors resulting from parameter and driver uncertainties at hourly and daily timescales at C flux tower sites operated within the Canadian Carbon Program (CCP). Furthermore, the magnitudes of errors resulting from the uncertainty assessments in a variety of parameter and driver fields are characterized to diagnose which errors contribute to the BEPS simulation performances. New phenology and nutrient release parameterization schemes are developed for the BEPS model to remove the common positive photosynthesis bias in winter, spring, and fall, observed by almost all ecosystem process models. This study complements the 1 km NPP mapping over Canada performed by *Liu et al*. [2002]. To our knowledge, high spatial resolution ecosystem process models used for global or regional simulations are typically operated at $0.5° \times 0.5°$ spatial resolution (of order 1500 km^2 averaged over Canada) at daily or hourly timescales although some studies have achieved simulations at 8 km [*Lafont et al*., 2012] and 1 km grid cell scales [*Liu et al*., 2002]. This study also extends the intercomparison of the daily and hourly BEPS models, which previous validation exercises have suggested perform comparably [*Liu et al*., 1997; *Chen et al*., 1999; *Liu et al*., 2002; *Sprintsin et al*., 2012]. The diagnostic error assessments and BEPS model intercomparisons are performed at CCP flux tower sites in order to optimize the mapping of Canada-wide GPP and NPP from daily BEPS simulations.

[8] Generally speaking, the objectives of this study are the assessment and mapping of GPP and NPP for Canada's entire land area at 250 m spatial resolution using BEPS model with new phenology and nutrient release parameterization schemes, improved key land surface input variables, and highly resolved parameterizations of photosynthesis and respiration rates.

2. Methods

2.1. Flux Data

[9] Observations of land surface C flux were made using the eddy covariance (EC) technique at nine forested sites in the CCP flux tower network [e.g., *Coursolle et al*., 2006]. The sites were selected based on the availability of key in situ data sets such as LAI, meteorology, and land surface C fluxes. Observations at EC towers have been used widely as the reference for land surface C flux measurements, relying on the assumption of a well-mixed, fully turbulent boundary layer above a relatively uniform and horizontal landscape at each site. The EC towers in the CCP network have "footprints" which vary in size, as a function of stand height, composition, surface roughness, and the meteorological conditions occurring at the time. More specifically, the CCP archive of EC data sets contains gap-filled [*Barr et al*., 2006] measurements of half-hourly net ecosystem CO_2 exchange (NEE) collected using a standardized protocol, as well as the corresponding meteorological and ancillary data (such as LAI) which can be used as input for BEPS model simulations.

[10] The nine sites include three distinct PFTs (Table 1). Data were selected from each site for 2008, being an optimal year for which the Canada-wide data sets are available for generating time series of LAI and other BEPS inputs such as clumping index [*He et al*., 2012], background surface reflectance [*Pisek and Chen*, 2009], and overstorey canopy LAI [*Gonsamo and Chen*, 2013]. From the half-hourly NEE data, we compute daily GPP sums following standard procedures [*Barr et al*., 2006]. Table 1 gives details of the nine CCP flux tower sites and the corresponding 90% flux footprint area [*Chen et al*., 2009, 2011].

Table 1. The Description of Studied Canadian Carbon Program (CCP) Flux Tower Sites[a]

Site	PFT	Latitude/ Longitude	Overstorey Genera	Age (2013)[b]	Maximum Overstorey LAI[b,c]	Mean Annual Temperature (°C)[b]	Mean Annual Precipitation (mm)[b]	V_m (μmol m^{-2} s^{-1})[d]	90% Flux Tower Footprint (km^2)[e,f]	Site References
SK OA	BDF	53.629/–106.198	*Populus*, *Corylus*	93	2.1	0.6	467	95.9	4	[*Barr et al*., 2004]
SK SOBS	BCF	53.987/–105.118	*Picea*	131	3.8	0.6	467	39.4	6.25	[*Bergeron et al*., 2007]
SK SOJP	BCF	53.916/–104.692	*Pinus*	96	2.6	0.6	467	56	6.25	[*Barr et al*., 2006]
BC DF49	TCF	49.867–125.334	*Pseudotsuga*	63	6.07	8.3	1461	54.1	4	[*Chen et al*., 2009]
BC DF88	TCF	49.535–124.900	*Pseudotsuga*	23	3.6	9.7	1179	38.8	0.25	[*Chen et al*., 2009]
BC DF00	TCF	49.871–125.291	*Pseudotsuga*	13	2.7	8.3	1461	20.5	0.5625	[*Chen et al*., 2009]
ON WPP39	TCF	42.710–80.357	*Pinus*	74	8	8.1	800	31	4	[*Arain and Restrepo-Coupe*, 2005]
QC EOBS	BCF	49.693/–74.342	*Picea*	106	3.7	0.0	961.3	32.3	4	[*Bergeron et al*., 2007]
QC HBS75	BCF	49.760/–74.571	*Picea*	38	2.6	0.0	961.3	32.3	4	[*Payeur-Poirier et al*., 2012]

[a]PFT = plant functional type, BDF = boreal deciduous forest, TCF = temperate coniferous forest, and BCF = boreal coniferous forest. The CCP flux tower sites include SK OA = Saskatchewan Old Aspen; SK SOBS = Saskatchewan Southern Old Black Spruce; SK SOJP = Saskatchewan Southern Old Jack Pine; BC DF49 = British Columbia Douglas-fir 1949; BC DF88 = British Columbia Douglas-fir 1988; BC = DF00 = British Columbia Douglas-fir 2000; ON = WPP39 = Ontario Turkey Point Mature White Pine Plantation 1939; QC EOBS = Quebec Eastern Old Black Spruce; and QC HBS75 = Quebec Harvested Black Spruce 1975.
[b]Canadian Carbon Program (CCP).
[c]*Chen et al*. [2006b].
[d]*Groenendijk et al*. [2011].
[e]*Chen et al*. [2009].
[f]*Chen et al*. [2011].

2.2. Ecosystem Models and Experimental Protocols

2.2.1. Daily BEPS

[11] Daily BEPS [*Liu et al*., 1997, 1999], hereafter referred as BEPSd, is a process-based two-leaf enzyme kinetic terrestrial ecosystem model designed to simulate energy, water, and C fluxes at daily time steps using spatial data sets of meteorology, remotely sensed land surface parameters (LAI, land cover type, and clumping index), soil water holding capacity (SWHC), and land cover-dependent parameters for photosynthesis and respiration rates [*Liu et al*., 2002]. Daily C fixation is calculated by scaling the Farquhar leaf biochemical model [*Farquhar et al*., 1980] up to the whole canopy level implemented with the spatial and temporal scaling schemes of *Chen et al*. [1999]. Daily GPP is calculated separately for sunlit and shaded leaves [*Liu et al*., 2002] after the analytical integration of the Farquhar model over each day to account for diurnal variations of meteorological variables on photosynthesis, through several steps of mathematical development [*Chen et al*., 1999; *Liu et al*., 1999]. More detailed descriptions of model structure, simulation of photosynthesis, plant respiration, and other biological processes are available in *Liu et al*. [1999]. C fixation in BEPSd is constrained by leaf stomatal conductance scaled by photosynthetic photon flux density, temperature (T), vapor pressure deficit, and leaf water potential [*Jarvis*, 1976].

2.2.2. Hourly BEPS

[12] Hourly BEPS [*Ju et al*., 2006; *Chen et al*., 2007], hereafter referred to as BEPSh, is an extended version of BEPSd designed to simulate instantaneous leaf-level photosynthesis and respiration. Compared to BEPSd, BEPSh includes a land surface scheme to calculate energy balance, sensible and latent heat fluxes, soil water, and soil temperature status [*Ju et al*., 2006; *Chen et al*., 2007]. The "Jarvis" model [*Jarvis*, 1976] used for the calculation of stomatal conductance in BEPSd is replaced by the Ball-Woodrow-Berry model [*Ball et al*., 1987].

[13] The two ecosystem models used in this study share the same general structure, allowing the description of the same biophysical processes. However, the ways the processes are represented differ greatly. BEPSh treats each time step calculation as instantaneous with no temporal integration but suffers from the need for, and inaccuracy of, spatial scaling due to computational demands needed for high spatial resolution simulation. BEPSd is suitable for high spatial resolution remote sensing applications because of its moderate demand on computation and input data. Since the diurnal variations of solar radiation, temperature, and the associated canopy processes generally follow predictable patterns, BEPSd, when correctly parameterized and temporally integrated, can capture most of the day-to-day variability in the plant canopies. Although both BEPSd and BEPSh have been through several validation exercises [*Liu et al*., 1997; *Chen et al*., 1999; *Liu et al*., 1999, 2002; *Chen et al*., 2007; *Schwalm et al*., 2010; *Chen et al*., 2012; *Schaefer et al*., 2012; *Sprintsin et al*., 2012; *Zhang et al*., 2012], no systematic comparison has been conducted previously between the two models. Key differences between BEPSd and BEPSh relevant for the current study are given in Table 2.

[14] NPP from both BEPSd and BEPSh is calculated as a difference of GPP and autotrophic respiration [*Ju et al*., 2006; *Liu et al*., 2002]. Autotrophic respiration is separated into maintenance respiration and growth respiration [*Running and Coughlan*, 1988]. Growth respiration is calculated as a proportion of GPP depending on respiration coefficient and carbon allocation fraction for each plant component (leaf, stem, and root). The maintenance respiration is temperature dependent and calculated as a product of biomass (sapwood for stems), maintenance respiration coefficient, and temperature sensitivity factor (Q_{10}) of each plant component. The

Table 2. Main Differences Between BEPSd and BEPSh[a]

	BEPSd	BEPSh
Time step	24 h	1 h
Meteorology input	Minimum temperature, maximum temperature, radiation, humidity, and precipitation	Temperature, radiation, humidity, precipitation, and wind
Soil input	Soil water holding capacity	Soil texture
Soil layer	1	5
Daily GPP	Integrated with day length factor	Sum of instantaneous simulation
Stomatal conductance	Jarvis	Ball-Woodrow-Berry
Vertical integration of N-weighted V_m	No	Yes
Vertical integration of N-weighted J_m	No	Yes
Soil temperature calculation	No	Yes
Moisture variable	Relative soil moisture from volumetric soil water and soil water holding capacity	Soil moisture scaling factor from root distribution, soil water content, and soil temperature
Coupling energy, water, and carbon exchange in the soil-vegetation-atmosphere system	Yes	Yes

[a]N is Nitrogen, J_m is maximum rate of electron transport, and V_m is maximum carboxylation rate of Rubisco.

respiration coefficients and carbon allocation fraction vary among land cover types [*Ju et al*., 2006; *Liu et al*., 2002; *Running and Coughlan*, 1988].

2.2.3. Model Parameterization and Forcing

2.2.3.1. Meteorological Observations

[15] In addition to the half-hourly data (including incoming shortwave radiation, air temperature, humidity, precipitation, and wind speed) obtained for each flux tower site, 6-hourly reanalysis data were obtained from National Centers for Environmental Prediction (NCEP) and interpolated temporally to produce hourly values. Different interpolation methodologies were used for the different variables. Specific humidity and wind speed were assumed to remain constant within each 6 h NCEP interval. Total precipitation was equally distributed across the 6 h interval. Incoming shortwave radiation was calculated for each hour as a function of the solar zenith angle and the 6 h total incoming shortwave radiation from NCEP. Hourly air temperature was determined from the 6 h data and daily maximum/minimum values also available in the NCEP data. The same data sets were also aggregated into daily meteorological input. The hourly and daily integrated NCEP data were then interpolated bilinearly to a 250 m grid for Canada-wide simulations. The half-hourly EC tower meteorology measurements were also aggregated into hourly and daily values for BEPSh and BEPSd simulations, respectively.

2.2.3.2. Land Cover Observations

[16] We have used a new 250 m North American Land Cover (NALC2005) product (www.cec.org). The NALC2005 classification was derived from a time composite from summer 2005 seven land bands of level 1B Moderate Resolution Imaging Spectroradiometer data (collection 5) and ancillary geographic information system layers following an enhanced classification method and classification by progressive generalization approaches [*Latifovic et al*., 2004]. Compared to the commonly used 1 km Global Land Cover (GLC2000) product, the 250 m NALC2005 has better quantitative accuracy over Canada based on reference data and visual and qualitative assessments [*Gonsamo and Chen*, 2011].

2.2.3.3. Canopy Structure Observations

[17] In preparation for 250 m GPP and NPP simulations over Canada, we have produced a 250 m spatial resolution LAI data set [*Gonsamo and Chen*, 2013]. The new LAI product makes an improved use of the University of Toronto (UofT) LAI algorithm which has previously been used to support global initiatives such as the European Space Agency Global Land Products for Carbon Model Assimilation project for global and climate change assessments [*Deng et al*., 2006]. The UofT LAI algorithm, based on the 4-Scale geometrical optical model [*Chen and Leblanc*, 1997], makes use not only of the surface reflectances in red, near infrared, and midinfrared of each pixel but also of the angular information at the time of data acquisition, including solar zenith angle, view zenith angle, and the difference between sun and satellite azimuth angles. Recent development [*Gonsamo and Chen*, 2013] includes further improvement of the UofT v2 LAI algorithm including enhanced spatial resolution (250 m) by considering a pixel-by-pixel 250 m land cover map, local topography (slope and aspect), clumping index, and background reflectance variations to produce overstorey LAI time series. To remove residual cloud and atmospheric effects in the 10 day LAI time series, we use a locally adjusted cubic-spline capping (LACC) method based on the seasonal trajectory of each pixel [*Chen et al*., 2006a]. Final canopy LAI is corrected using the foliage clumping index obtained independently from multiangle remote sensing observations [*He et al*., 2012]. This unique approach is compatible with the need for accurate separation of sunlit and shaded leaves, which requires not only the LAI but also clumping index. The pixel-by-pixel clumping index is also an independent input datum for both BEPS models. We further compiled in situ maximum summer time overstorey (canopy) LAI from literature (CCP data archive) [*Chen et al*., 2006a, 2006b] for BEPS simulations using solely in situ LAI time series. Since the in situ LAI measurements are collected for a single date, during the peak of the growing season, we used the scaled UofT LAI time series to produce in situ time series. The scaling is conducted as a product of the ratio of the in situ to the summer time maximum UofT LAI multiplied by the UofT LAI time series. This scaled product is considered as a reference LAI time series, since the temporal trajectory is captured using an LACC temporal smoothing method applied to the UofT LAI product.

2.2.3.4. Soil Property Observations

[18] For BEPSd, the required soil observation is the SWHC used to calculate the soil water balance using a one-layer bucket model and derived from the coarse material content, soil texture, and maximum root depth spatial data of the Soil Landscape of Canada (SLC v1.0) database [*Liu et al*., 2002]. For BEPSh, soil texture information was used to estimate hydrological parameters including porosity, field capacity (water potential at 33 kPa), wilting point (water potential at

Table 3. Revised Photosynthesis Parameters Used for GPP and NPP Simulation Over Canada

Parameter	Temperate Conifer Forest	Boreal Conifer Forest	Boreal Broadleaf Forest	Mixed Forest	Shrub	Temperate Grassland	Crop	Tundra, Bog, Marsh, and Grass
Maximum stomatal conductance: g_{max} ($mm\,s^{-1}$)[a,b]	1.6	1.6	5	3	5	5	5	5
Maximum carboxylation at 25°C: V_m ($\mu mol\,m^{-2}\,s^{-1}$)[c,d]	33.9	33.9	95.9	41.5	33	57.4	105.2	33
Specific leaf area: SLA ($m^2\,kg\,C^{-1}$)[e,f]	12[f]	10	25	18	—	—	—	—

[a] *Chen et al*. [1999].
[b] *Liu et al*. [2002].
[c] *Groenendijk et al*. [2011].
[d] *Bubier et al*. [2011].
[e] *Middleton et al*. [1997].
[f] *Weiskittel et al*. [2008].

1500 kPa), saturated hydraulic conductivity, and air entry water potential. These parameters were used to calculate a soil water scaling parameter to determine the hydraulic and physical properties of the soil layers [*Ju et al*., 2006]. For individual EC tower sites, site-level soil texture data were obtained from the CCP flux measurement databases of ancillary site data.

2.2.3.5. Photosynthesis Parameter Observations

[19] Several biophysical and biochemical rate parameters are needed to simulate photosynthesis and respiration in both BEPSd and BEPSh. Key parameters are given in Table 3. The main focus in this study lies in V_m (leaf-level maximum carboxylation rate at 25°C in $\mu mol\,m^{-2}\,s^{-1}$) which is a common key parameter in both BEPS models. This single parameter represents the maximum rate of carboxylation by the photosynthetic enzyme Rubisco, the maximum rate of electron transport (J_m), and the scaling of leaf maintenance respiration. However, estimates of V_m vary greatly, and the range of possible values is large, even within a single PFT [e.g., *Farquhar et al*., 1980; *Beerling and Quick*, 1995; *Chen et al*., 2012; *Sprintsin et al*., 2012]. A recent study by *Groenendijk et al*. [2011] shows substantial variation of V_m even at individual flux tower sites. We use the flux data to evaluate sensitivity of simulated GPP to the effect of varying V_m. In this study, site level V_m for each site is listed in Table 1, and the land cover-averaged values are listed in Table 3 which is eventually used for Canada-wide GPP and NPP simulations.

2.2.3.6. Phenology and Nutrient Release Parameterization

[20] Leaf phenology remains one of the most difficult ecosystem processes to parameterize in terrestrial ecosystem models because our understanding of the underlying physiological processes that initiate leaf onset and senescence is incomplete. Recent findings show the strong need for better representation of phenology in terrestrial models [*Arora and Boer*, 2005; *Richardson et al*., 2011]. In BEPS, the timing of onset and senescence of leaf phenology are represented by actual seasonal progression of LAI. However, the phenology of photosynthesis and nutrient availability is often overlooked in many studies and also needs better representation. A recent model data intercomparison from the North American Carbon Program (NACP) site synthesis showed that most ecosystem models overestimate GPP during low-temperature periods in winter, spring, and fall [*Schaefer et al*., 2012]. Photosynthesis in many terrestrial ecosystems is further limited by nutrients, predominantly nitrogen (N) and phosphorus (P), in addition to other environmental constraints such as water, light, and temperature. Nutrient availability for plants is quite sensitive to biochemical P and N mineralization and immobilization, which usually follow changes in soil and air temperatures in seasonally frozen ecosystems as does microbial activity [e.g., *Schmidt et al*., 1999; *Contosta et al*., 2011]. Building on recent work by *Gonsamo et al*. [2012a, 2012b] to develop empirical representations of photosynthesis and carbon uptake phenology for Canadian forests and on the results reported by *Schaefer et al*. [2012], we have developed a new phenology and nutrient release function ($f_{p,n}$) to be used for BEPS in temperate, boreal, and Arctic Canada.

[21] For hourly BEPS (BEPSh)

$$f_{p,n} = \begin{cases} 0 & \text{if } T\text{air and } T\text{soil} \le 0 \\ \dfrac{1}{\left[\left(\dfrac{5 - T\text{air}}{5}\right) + 1\right]} \times \dfrac{1}{\left[\left(\dfrac{190 - \text{DOY}}{190}\right) + 1)\right]} & \text{if } T\text{air} \le 5 \text{ and DOY} \le 190 \\ \dfrac{1}{\left[\left(\dfrac{190 - \text{DOY}}{190}\right) + 1\right]} & \text{if } T\text{air} > 5 \text{ and DOY} \le 190 \\ \dfrac{1}{\left[\left(\dfrac{5 - T\text{air}}{5}\right) + 1\right]} & \text{if } T\text{air} \le 5 \text{ and DOY} > 190 \end{cases} \quad (1)$$

Table 4. BEPS Simulation Protocols

Simulation	Error Sources	Description
Measurement	N/A	**Reference measure**
BEPS-site	Model structural error	**Control simulation** with site parameter (V_m), site meteorology (temperature, radiation, wind, precipitation, and humidity), and site LAI
BEPS-MET	Model driver (meteorology) uncertainty	Simulation with NCEP meteorology (temperature, radiation, wind, precipitation, and humidity), site parameter (V_m), and site LAI
BEPS-LAI	Model driver (LAI) uncertainty	Simulation with site meteorology (temperature, radiation, wind, precipitation, and humidity), site parameter (V_m), and UofT MODIS LAI
BEPS-V_m	Model parameter (V_m) uncertainty	Simulation with site meteorology (temperature, radiation, wind, precipitation, and humidity), land cover-averaged (V_m), and site LAI
BEPS-scene	Combined model structural error, parameter, and driver uncertainties	Canada-wide simulation with optimized NCEP meteorology (temperature, radiation, wind, precipitation, and humidity), land cover-averaged parameter (V_m), and corrected UofT MODIS LAI

[22] For daily BEPS (BEPSd)

$$f_{p,n} = \begin{cases} 0 & \text{if } T\max \le 0 \\ \dfrac{1}{\left[\left(5 - \dfrac{\{T\max + T\min\}}{2}\right) + 1\right]\left[\left(\dfrac{190 - \mathrm{DOY}}{190}\right) + 1\right]} & \text{if } \dfrac{(T\max + T\min)}{2} \le 5 \text{ and DOY} \le 190 \\ \dfrac{1}{\left[\left(\dfrac{190 - \mathrm{DOY}}{190}\right) + 1\right]} & \text{if } \dfrac{(T\max + T\min)}{2} > 5 \text{ and DOY} \le 190 \\ \dfrac{1}{\left\{\left[5 - \dfrac{(T\max + T\min)}{2}\right] + 1\right\}} & \text{if } \dfrac{(T\max + T\min)}{2} \le 5 \text{ and DOY} > 190 \end{cases} \quad (2)$$

$f_{p,n}\left\{1/\left[\left(\frac{190 - \mathrm{DOY}}{190}\right) + 1\right]\right\}$ is a "Monod" type equation, where the Monod employs an arbitrary value for the specific curve rate. Here we use air temperatures (for BEPSh: $1/\left[\left(\frac{5 - T\mathrm{air}}{5}\right) + 1\right]$) and (for BEPSd: $1/\left\{\left[\frac{5 - \frac{(T\max + T\min)}{2}}{5}\right] + 1\right\}$) to determine the specific curve rates of nutrient release and photosynthesis phenology. Following the common practice of EC measurements for GPP and recent findings from the NACP model-data intercomparison [*Schaefer et al.*, 2012], GPP is shut down when soil and air temperatures are both below zero for BEPSh, and when the daily maximum air temperature is below zero for BEPSd. Finally, we use simple multiplicative and threshold formulations of $f_{p,n}$, both of which are dependent on the day of year (DOY) and soil and air temperatures to produce the corrected GPP:

$$\mathrm{GPP} = f_{p,n} \times \mathrm{GPP} \quad (3)$$

2.2.4. Experimental Protocols for Diagnostic Error Assessment

[23] Data-oriented diagnostic techniques provide a means to evaluate uncertainties in the driving variables and parameters, as well as potential errors in model equations. Here we use the EC C flux, meteorology, LAI, and V_m observations to evaluate forcing and parameterization schemes in BEPS simulations. We investigate biases in GPP arising from the model's representation of processes (termed model structural error), from uncertainty in a key model photosynthetic parameter (termed model parameter uncertainty), and from uncertainty in key model drivers (termed model driver uncertainty) (Table 4).

[24] Model structural error indicates deficiencies in model equations and process representations as a model performance is evaluated after a run that has been constrained with measured in situ parameter and driver fields. We performed five simulations to document biases arising from different potential causes of error (Table 4). The last of these five simulations was denoted BEPS-scene to distinguish the full Canada-wide simulation performance by use of optimized driver and parameter fields from the other site-level simulations. Optimizations of parameter and driver inputs were carried out independently of the model simulations. For example, optimization of radiation input requires that scene level (NCEP) radiation input is regressed against the in situ radiation measurements in order to derive a radiation correction coefficient [*Liu et al.*, 1997, 2002] irrespective of the impact of NCEP data in BEPS simulations. The site-level values for V_m and LAI are given in Table 1, and site meteorology is from flux tower measurements. The nonoptimized

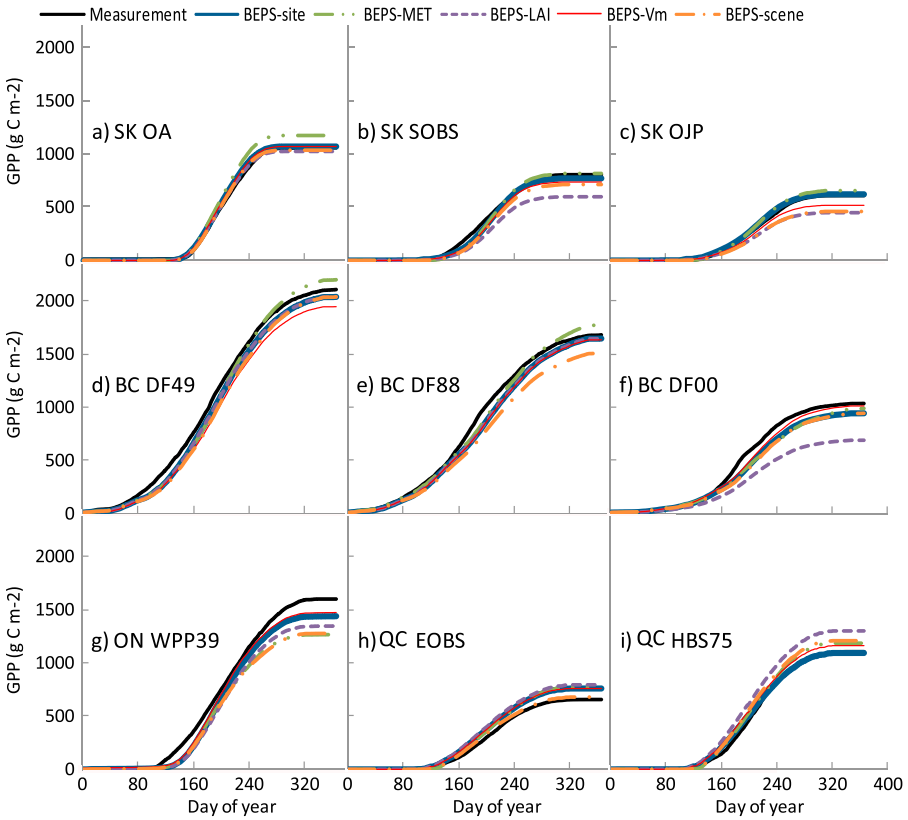

Figure 1. Comparisons of accumulated GPP profiles for year 2008 across nine Canadian Carbon Program (CCP) flux tower sites simulated at daily timescale using daily BEPS (BEPSd) model (see Table 4 for explanation of BEPS simulation protocol corresponding to each plotted line).

simulations are conducted using land cover-averaged V_m (Table 3), the UofT LAI product, and NCEP meteorology. All BEPS simulations were conducted for the corresponding 90% flux footprint area (Table 1).

2.3. Statistical Methods Used for Evaluating and Comparing Model Performances

[25] To evaluate the accuracy and determine the levels of errors of the BEPS experimental simulations, we followed commonly used model intercomparison approaches, including the Pearson correlation coefficient (r), estimates of errors in the form of root-mean-square-error (RMSE), and biases in the simulated values. According to statistical conventions, a t value greater than the critical value for $p = 0.05$ (two tailed, t test) was used to indicate that the simulation showed a significant bias toward overestimation or underestimation when compared with measured values.

[26] The interdiurnal variability within BEPS simulations and measured values were evaluated using a normalized sensitivity function [*Gonsamo*, 2011]:

$$N_X^Y = \frac{\bar{Y}}{\bar{X}} \lim_{\Delta X \to 0} \frac{dY}{dX} \cong \frac{\Delta Y}{\Delta X} \frac{\bar{Y}}{\bar{X}} = \frac{\Delta lnY}{\Delta lnX} \quad (4)$$

where $\bar{X}$ is the average value of factor X and $\bar{Y}$ is the average value of factor Y between day ($_i$) and ($_i + 1$). In the case of GPP, Y represents the value simulated by BEPS, and X is the observed value. If the measured interdiurnal variation of GPP is captured in simulated GPP, then N_X^Y equals 1. The normalized sensitivity function N_X^Y can be interpreted as the percentage change in Y for a 1% increase in X. We plotted the interdiurnal variability of simulated GPP (ΔlnY) against the interdiurnal variability of measured GPP (ΔlnX). Finally, as a complement to the statistical methods described above, the seasonal variation in GPP was analyzed by plotting model simulations compared to site measurements.

3. Results

3.1. Diagnostic Error Assessment at Daily Timescales

[27] Figures 1 and 2 present the cumulative GPP as simulated using BEPSd and BEPSh, respectively, following the five experimental protocols (Table 4) together with the measured GPP at nine flux tower sites. BEPS-site simulations from both BEPSd and BEPSh compare most favorably with measured GPP, with daily absolute average bias of less than 3%. LAI is the main source of error for BEPS simulations followed by V_m, with meteorology causing the least uncertainty. BEPSd is affected less by parameter and driver uncertainties than BEPSh. Once the parameters and drivers were optimized, i.e., the results from BEPS-scene, their interaction effect still remains large although the all-site-averaged results show small overall errors (Table 6). The errors from parameter and driver fields generally interact to counteract or enhance the variations in simulated GPP from the optimized BEPS-scene experimental protocol compared to the measured values. Both BEPSd and BEPSh capture the seasonal trajectories of

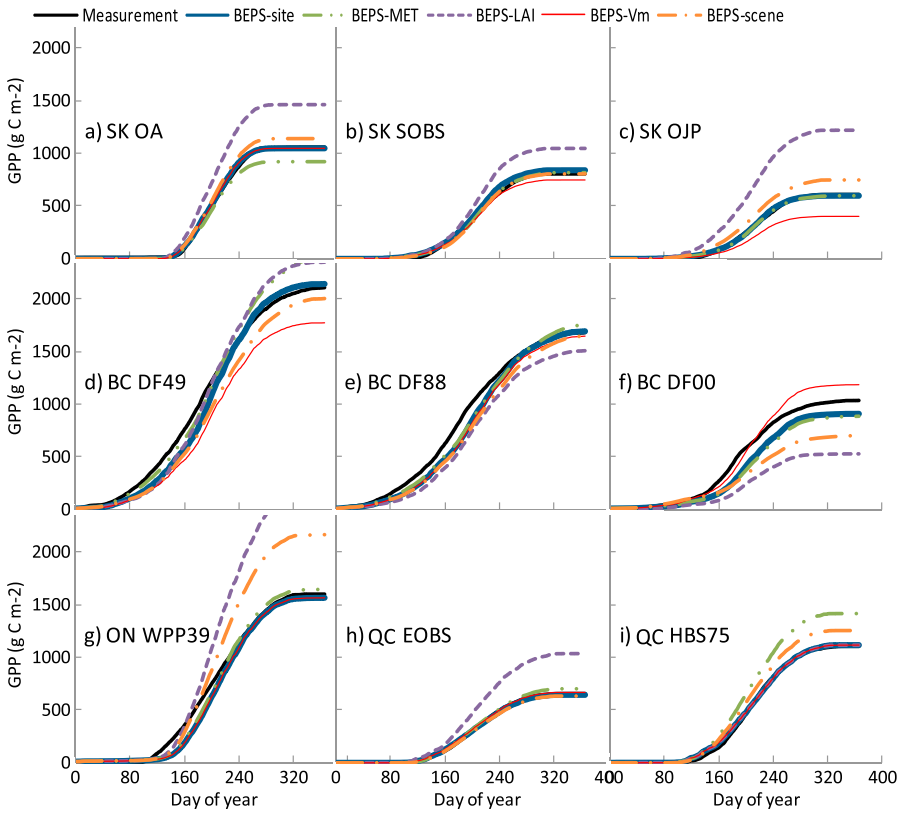

Figure 2. Comparisons of accumulated GPP profiles for year 2008 across nine Canadian Carbon Program (CCP) flux tower sites simulated at hourly timescale using hourly BEPS (BEPSh) model (see Table 4 for explanation of BEPS simulation protocol corresponding to each plotted line).

GPP at all flux tower sites (Figures 1 and 2). Among the meteorology drivers, shortwave radiation is the major cause of simulation-to-measurement disagreement (not presented here for brevity), but this can be explained to some extent by large differences between the NCEP data and those measured at the EC tower sites. The comparison of measured and NCEP radiation shows that NCEP radiation overestimates the measured site level data by 54%, with a comparable result reported by *Liu et al*. [1997]. Furthermore, comparison of measured and NCEP observations shows that NCEP overestimates maximum temperature by −1.9%, minimum temperature by 6.3%, and humidity by −2.3%. We speculate this is due to the NCEP data set neglecting the effects of radiation absorption by aerosols. Therefore, when we simulate GPP and NPP using BEPS-scene parameters and input data, which is eventually used for Canada-wide NPP mapping, the radiation is adjusted by multiplying by 0.65. The same correction approach, based on multipliers derived from measured site level and Canada-wide input data comparisons, was used to optimize all driver and parameter fields for BEPS-scene simulations.

[28] BEPS-site simulations of GPP show statistically significant bias for only three flux tower sites in the case of BEPSd and only one for BEPSh (Table 5). This indicates that the hourly BEPS model, given accurate input parameter and drivers, will result in better GPP estimates. The site level statistics (Table 5) show the contributions of errors due to LAI, meteorology, and V_m are more prominent for BEPSh than for BEPSd indicating that BEPSh is more affected by errors in the input parameter and driver fields than BEPSd.

[29] The assessment of interdiurnal variability presented in Figure 3 further reveals that measured GPP shows higher interdiurnal variability than the simulations with BEPSd using either in situ or NCEP meteorology data. However, both BEPSd and BEPSh capture much of the measured interdiurnal variability (see statistically significant nonzero regression slopes in Figure 3). Much higher R^2 between BEPSh and measured GPP interdiurnal variability indicates that BEPSh captures this variability significantly better than BEPSd with regression slopes also much closer to unity in Figures 3c and 3d. Despite the fact that BEPSh is more affected by input parameter and driver errors (Figure 2 and Table 5), when used with site level measured inputs (BEPS-site), it outperforms BEPSd in capturing the interdiurnal variability (Figure 3), seasonal trajectories (Figure 2), and the overall magnitude of GPP (Table 5).

3.2. BEPS Performance Assessment for Canada-Wide Simulation

[30] Summary statistics for all five experimental protocols averaged for all flux tower sites are given in Table 6. On average, the BEPS-site simulations underestimated GPP by 2.7% (BEPSd) and by 1.1% (BEPSh), indicating better performance of BEPS models when in situ meteorology; V_m and LAI data sets were used. The coefficient of variation (CV) from measured GPP was 1.08, whereas from all five experimental protocols of both BEPSd and BEPSh ranged from 1.08 to 1.23 indicating that the measured variability of GPP is captured reasonably well by both models. The results

Table 5. Total Simulation Errors (RMSE) Across All CCP Sites in GPP (g C m^{-2} d^{-1})[a]

	Daily BEPS Model					Hourly BEPS Model				
Site	BEPS-Site	BEPS-MET	BEPS-LAI	BEPS-V_m	BEPS-Scene	BEPS-Site	BEPS-MET	BEPS-LAI	BEPS-V_m	BEPS-Scene
SK OA	1.06(↔)	1.04(↑)	1.01(↔)	1.06(↔)	0.97(↔)	1.04(↔)	1.26(↓)	1.41(↑)	1.04(↔)	1.26(↑)
SK SOBS	1.05(↔)	1.15(↔)	0.9(↓)	1.05(↓)	0.94(↓)	0.99(↔)	1(↔)	1.27(↑)	0.89(↓)	0.99(↔)
SK SOJP	0.64(↔)	0.61(↑)	0.49(↓)	0.59(↓)	0.45(↓)	0.75(↔)	0.72(↔)	1.28(↑)	0.53(↓)	0.7(↑)
BC DF49	1.96(↔)	1.88(↑)	1.96(↔)	1.71(↓)	1.77(↔)	2.37(↔)	2.2(↑)	2.49(↑)	1.98(↓)	2.01(↓)
BC DF88	1.53(↔)	1.56(↑)	1.53(↔)	1.52(↔)	1.33(↓)	1.84(↔)	1.71(↑)	1.7(↓)	1.8(↔)	1.74(↔)
BC DF00	1.11(↓)	0.99(↔)	0.76(↓)	1.18(↔)	1.16(↓)	1.41(↓)	1.38(↓)	0.87(↓)	1.71(↑)	0.93(↓)
ON WPP39	1.7(↓)	1.55(↓)	1.63(↓)	1.71(↓)	1.55(↓)	2.01(↔)	2.21(↔)	2.99(↑)	2.01(↔)	2.57(↑)
QC EOBS	0.83(↑)	0.83(↑)	1(↑)	0.84(↑)	0.87(↔)	0.61(↔)	0.75(↑)	1(↑)	0.62(↔)	0.67(↔)
QC HBS75	1.31(↔)	1.41(↑)	1.62(↑)	1.42(↔)	1.51(↑)	1.2(↔)	1.63(↑)	1.2(↔)	1.2(↔)	1.46(↑)

[a]Nature of statistically significant simulation biases ($p < 0.05$, two tailed, t test): ↔, no bias; ↑, overestimation; ↓, underestimation.

from the CV analysis are consistent with the results obtained from interdiurnal variability assessments (Figure 3). Overall, BEPS-site shows higher correlation and less bias (Figure 4). It is also evident that LAI is one of the main sources of driver error among the considered parameter and driver fields (Table 6). Using the in situ, LAI reduced the absolute bias in GPP from 7.3% to 2.7% and from 20.7% to 1.15% for BEPSd and BEPSh simulations, respectively.

[31] Our main goal of conducting diagnostic error assessments was to optimize the inputs for Canada-wide GPP and NPP simulations using BEPS. The performance of the BEPSd simulation for Canada-wide mapping is shown in Figure 4a (results obtained using BEPS-scene). The overall bias for BEPS-scene evaluated at nine flux tower sites are −7.56% for BEPSd (Figure 4a) and 1.17% for BEPSh (Figure 4b). However, BEPSd optimized for Canada-wide simulation shows a smaller spread of error indicated by relatively lower RMSE (Figure 4a) compared to BEPSh (Figure 4b), which can be attributed to BEPSd being less affected by errors from parameter and driver fields, hence making it more suitable for large scale GPP and NPP simulations. The reduced error distribution is a key trait to capture the correct spatial, interdiurnal, and seasonal distributions of GPP, and hence of NPP, for large-scale simulation. The required number of measurable inputs, the computing resources and processing time for Canada-wide simulation, is also lower for BEPSd compared to BEPSh. Therefore, we use BEPSd (BEPS-scene) to generate the 250 m resolution Canada-wide GPP and NPP maps discussed in the following section.

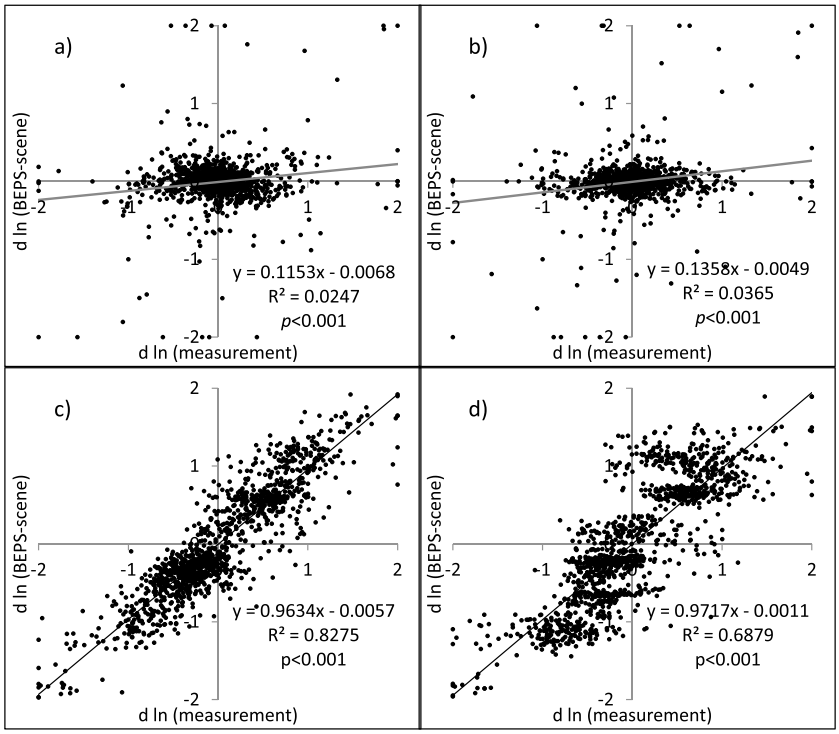

Figure 3. The proportional interdiurnal changes between the simulated GPP (Y axis) and measured GPP (X axis). (a) and (b) From daily BEPS simulations using in situ measured (BEPS-site) and Canada-wide optimized (BEPS-scene) inputs, respectively. (c) and (d) From hourly BEPS simulations using in situ measured (BEPS-site) and Canada-wide optimized (BEPS-scene) inputs, respectively. If the regression slope is a unity, the simulation proportionally explains the measured interdiurnal variation of GPP.

Table 6. All-Site-Averaged Summary Statistics for Measured and Simulated GPP[a]

BEPS Simulations	*a*	*b*	*r*	RMSE	Bias
		Daily BEPS			
BEPS-site	0.23	0.90	0.92	1.35	−0.09
BEPS-MET	0.25	0.94	0.92	1.40	0.05
BEPS-LAI	0.16	0.88	0.91	1.44	−0.24
BEPS-V_m	0.22	0.90	0.92	1.33	−0.11
BEPS-scene	0.16	0.88	0.92	1.32	−0.25
		Hourly BEPS			
BEPS-site	0.02	0.98	0.92	1.51	−0.04
BEPS-MET	0.24	0.97	0.90	1.63	0.14
BEPS-LAI	0.08	1.18	0.87	2.40	0.67
BEPS-V_m	0.05	0.93	0.91	1.49	−0.16
BEPS-scene	0.16	0.99	0.89	1.81	0.13

[a]Measured GPP = *a*(simulated GPP) + *b*; *a*, regression intercept; *b*, regression slope; *r*, Pearson correlation coefficient; RMSE, root-mean-square-error. RMSE and bias are presented in g C m^{-2} d^{-1}.

3.3. GPP and NPP Distribution Over Canada

[32] Figure 5 presents Canadian maps of total GPP and NPP estimated using BEPSd following the BEPS-scene protocol at 250 m spatial resolution for 2008, together with maps of mean annual LAI and land cover. A reasonable spatial agreement is found among the simulated C fluxes (GPP and NPP), LAI, and land cover. Simulated values of GPP exceeding 2 kg C m^{-2} y^{-1} and of NPP exceeding 1 kg C m^{-2} y^{-1} occurred in very few pixels. Fifty percent of Canada's land area had simulated values below 0.38 kg C m^{-2} y^{-1} (GPP) and 0.18 kg C m^{-2} y^{-1} (NPP). Simulated GPP was generally highest in the temperate and southern boreal regions, but NPP formed a higher fraction of GPP in forested regions of the boreal zone than elsewhere (Figure 5).

[33] The values of GPP and NPP simulated by BEPS depended greatly on land cover types and ecozones (Table S1 in the supporting information and Table 7). The Boreal Plains, Pacific Maritime, Atlantic Maritime, and Mixedwood Plains ecozones had comparably higher NPP (generally exceeding 300 g C m^{-2} y^{-1}) due to their large proportion of forested areas and more southerly extents. Atlantic Maritime ecozone consisting of Prince Edward Island, Nova Scotia, New Brunswick, and southeastern Quebec provinces was simulated to have annual NPP comparable to that of the Pacific Maritime ecozone, which is dominated by highly productive temperate evergreen forests in British Columbia and less productive forests in the southwestern Yukon Territory. The lowest NPP was obtained in the Arctic ecozones. NPP distribution also greatly varied by provinces, Nunavut having the lowest NPP. Detailed statistics of GPP based on provinces, cover types, and ecozones are given in Table S1.

[34] The Canada-wide analysis indicates that deciduous forest has the highest mean NPP followed by coniferous forest and mixed forest. Among nonforested areas, agricultural crops generally have higher NPP. The area-weighted mean annual NPP (GPP) for forested land of Canada in 2008 was estimated to be 247 (533) g C m^{-2} y^{-1} totalling 1.02 (2.2) Pg C y^{-1}. Nonforested vegetation had mean annual NPP of 68 g C m^{-2} y^{-1} and total NPP of 0.25 Pg C y^{-1}.

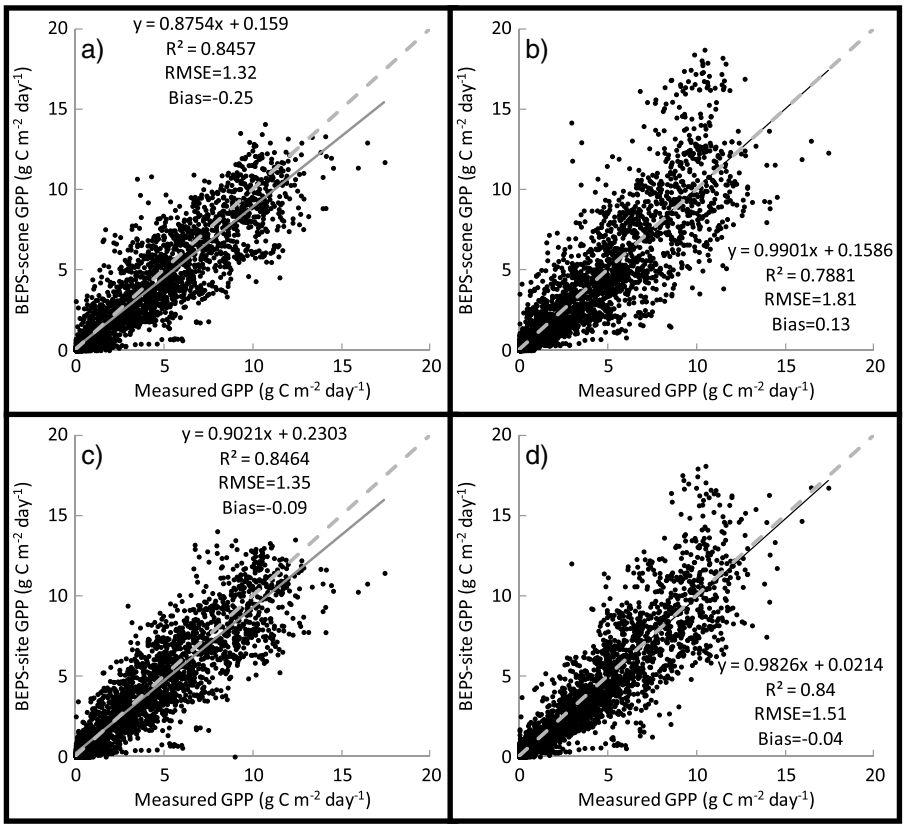

Figure 4. Scatterplots of (a) and (b) simulated (BEPS-scene) and measured GPP from daily and hourly timescale models used for Canada-wide mapping of GPP. (c) and (d) BEPS-site simulations from daily and hourly timescale models, respectively. Bold is a regression line and broken is a 1:1 line.

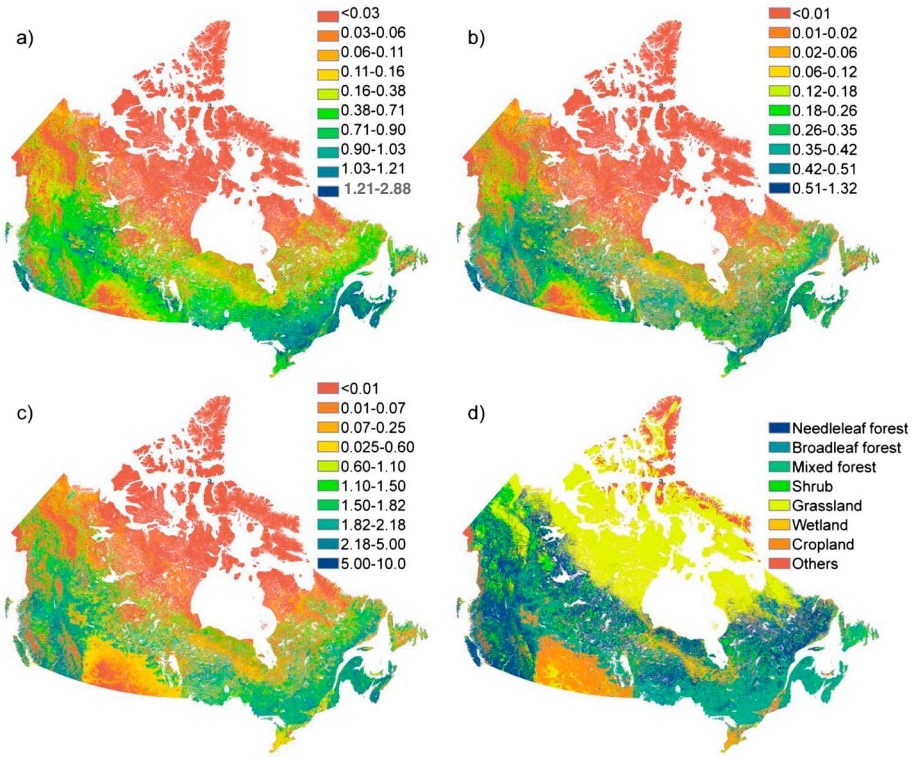

Figure 5. (a) Canada-wide 250 m spatial resolution maps of GPP (kg C m^{-2} y^{-1}), (b) NPP (kg C m−2 y−1), (c) overstorey mean leaf area index (LAI), and (d) land cover. GPP, NPP, and LAI are for 2008, and the land cover map is for 2005. GPP, NPP, and LAI are mapped in 10 quantile classes. GPP and NPP maps are from BEPSd simulations.

Hence, the national mean and total NPP were 164 g C m^{-2} y^{-1} and 1.27 Pg C y^{-1}, respectively. The national mean and total GPP were 344 g C m^{-2} y^{-1} and 2.68 Pg C y^{-1}, respectively. Based on the post-IBP (International Biological Programme) literature survey, the 95% confidence interval of global NPP estimates are 36.3–80.1 Pg C y^{-1} [*Ito*, 2011]. Accordingly, Canada's vegetation contributes 1.7%–3.5% of global NPP, although it composes 6.1% of the global terrestrial land surface area.

4. Discussion and Conclusions

[35] As shown in Figures 1 and 2 and Tables 5 and 6, BEPS proved highly affected by uncertainties in the values

Table 7. NPP by Ecozone, Province and Territory, and Land Cover Over Valid Land Pixels of Canada

Ecozone[a] (1000 km^2)	Mean NPP (SD) (g C m^{-2} y^{-1})	Province/Territory (1000 km^2)	Mean NPP (SD) (g C m^{-2} y^{-1})	Land Cover[b] (1000 km^2)	Mean NPP (SD) (g C m^{-2} y^{-1})
Arctic Cordillera (39)	3 (26)	Alberta (632)	273 (202)	Coniferous forest (2574)	230 (188)
Atlantic Maritime (195)	362 (204)	British Columbia (807)	285 (190)	Deciduous forest (440)	446 (204)
Boreal Cordillera (410)	118 (134)	Manitoba (554)	177 (179)	Mixed forest (1135)	207 (184)
Boreal Plains (670)	309 (202)	New Brunswick (71)	341 (195)	Shrub (689)[c]	48 (103)
Boreal Shield (1690)	250 (202)	Newfoundland and Labrador (356)	166 (179)	Grass (2403)[d]	39 (100)
Hudson Plains (364)	124 (146)	Northwest Territories (982)	63 (122)	Crop (539)	226 (167)
Mixedwood Plains (109)	366 (193)	Nova Scotia (51)	356 (215)	Urban (8)	26 (106)
Montane Cordillera (430)	294 (176)	Nunavut (1017)	2 (12)		
Northern Arctic (632)	0 (0)	Ontario (922)	246 (198)		
Pacific Maritime (159)	353 (215)	Prince Edward Island (5)	389 (182)		
Prairie (452)	156 (145)	Quebec (1370)	179 (204)		
Southern Arctic (685)	7 (29)	Saskatchewan (593)	167 (170)		
Taiga Cordillera (206)	55 (93)	Yukon Territory (428)	80 (116)		
Taiga Plains (568)	145 (177)				
Taiga Shield (1180)	76 (120)				
Canada forest (4149)	247 (200)				
Canada land (7788)	164 (193)				

[a] *Wiken* [1986].
[b] *Gonsamo and Chen* [2011]. NPP and total area are calculated for only valid land pixels.
[c] Shrub includes shrubland with lichen and moss.
[d] Grass includes wetland, grassland with lichen and moss, and barren land with lichen and moss. SD is standard deviation.

of parameter and drivers. For example, the use of in situ LAI instead of Canada-wide LAI product reduced simulation biases from −7.3% to −2.7% and from 20.7% to −1% for daily and hourly simulations, respectively. These results signify how much diagnostic error assessment may help understand error sources due to input data and parameters and due to structural errors in process-based models in general. Errors in input data (notably LAI and meteorology spatio-temporal time series), were generally larger than errors in the key V_m parameter in site-level comparisons. The likely range of physiological parameters is well constrained locally by measurements of C flux, while the meteorological data were conditioned on patchy, spatially dispersed data and large-scale estimates of LAI derived from optical satellite data were prone to contamination and interferences from cloud, signal saturation in dense canopies, and understorey vegetation.

[36] BEPSh has proven to be less biased than BEPSd. Of the nine EC flux tower sites listed in Table 5, only one simulation with BEPSh showed statistically significant bias compared to three simulated with BEPSd. This can be explained by the better coupling of C fluxes in the soil-vegetation-atmosphere continuum when using BEPSh [*Ju et al*., 2006] and by its more robust calculation of stomatal conductance. In contrast to BEPSd, the instantaneous hourly calculations of photosynthesis in BEPSh are less affected by temporal scaling of meteorological factors which have nonlinear effects on the photosynthesis rate. Some of the significant biases observed in BEPS-site simulations after using in situ meteorology, V_m and LAI, show the model structural error to the level of known driver and parameter fields we managed to constrain. General conclusions about the overall BEPS performances can only be inferred after constraining all rate and driver fields using as many known and measured inputs. However, recent BEPS simulations [*Liu et al*., 1999, 2002; *Ju et al*., 2006; *Chen et al*., 2012; *Sprintsin et al*., 2012; *Zhang et al*., 2012] and overall model-data comparisons of several enzyme kinetic (EK) and light use efficiency (LUE) models [*Schwalm et al*., 2010; *Schaefer et al*., 2012] show that BEPS performs comparably better than most of the considered models in simulating C flux. The study by *Schaefer et al*. [2012] also shows that none of the EK or LUE models using either the two-leaf or big-leaf approach match measured GPP within the range of uncertainty of observed fluxes. In the present study, the comparison of annual measured and simulated GPP using the BEPS-site and BEPS-scene protocols from both BEPSd and BEPSh models show that the mean differences between simulated and measured GPP are not statistically significant ($p > 0.05$, paired t test).

[37] The new phenology and nutrient release parameterization schemes applied in BEPSd and BEPSh removed the common positive biases (Figures S1 and S2 in the supporting information) in winter, spring, and fall, observed in many ecosystem models [*Schaefer et al*., 2012]. Part of this improvement likely resulted from the partitioning algorithm for the measured GPP flux, which also set GPP to zero when soil and the air temperatures are both below 0°C. Temperature is the dominant control of the seasonal variation in GPP at boreal sites. A BEPS based phenology sensitivity analysis shows that a variation of ±10 days in bud-burst dates led to a variation of ±5.0% for annual GPP [*Migliavacca et al*., 2012]. The new phenology and nutrient release parameterization schemes and the low-temperature inhibition function have reduced the simulated GPP error during winter and spring (January–May) and fall (September–December) from 18.5% to −7.6 and from 19% to −9% for daily and hourly simulations, respectively (Figures S1 and S2).

[38] Young stands such as BC DF88 and BC DF00 show rapid increase and decrease of GPP in early spring and late fall, respectively, which could not be successfully captured in BEPSd and BEPSh simulations (Figures 1 and 2). One possible reason is, as these sites are plantations after clear-cutting, rapid understorey leaf flushing from the opening between young tree crowns or the surrounding area may be the major part of rapid increase and decrease of GPP in early spring and late fall, respectively. In BEPS, understorey LAI is estimated as a function of overstorey LAI which makes it challenging to capture the dynamics across all forest ages and density classes. For example, at the peak of the growing season, deciduous understorey LAI contributed 98% of total LAI at the BC DF00 site (CCP data archive) and 46% at the QC HBS75 site [*Payeur-Poirier et al*., 2012].

[39] LAI has been shown to be an important driver because all leaf-level photosynthesis estimates must be scaled to the canopy level using the sunlit/shaded LAI values. Remote sensing of land surface parameters including LAI is still an evolving field [e.g., *Pfeifer et al*., 2012]. Although we have used an improved 250 m LAI product [*Gonsamo and Chen*, 2013], estimation of overstorey LAI remains challenging.

[40] One of the main reasons that V_m did not show significant effect on most sites both for BEPSd and BEPSh simulations is that we used the 250 m regional land cover map for site-level GPP comparisons where each pixel is a single vegetation type. As such, each site albeit dominated by its major vegetation type can still have significant proportion of other land cover types in its respective flux footprint area. When the V_m is changed to a site specific value, the V_m values of other land covers types within each flux footprint area are kept with the one used for Canada-wide simulation (averaged values per land cover). Therefore, only pixels which are labeled as the flux tower site specific land cover type are assigned site-specific V_m in the respective footprint of each flux tower site.

[41] One of the applications of this study would be to replace a reference NPP measure used in Canada-wide mapping of landmass C source and sink distribution [*Chen et al*., 2003] as implemented in an Integrated Terrestrial Ecosystem C-budget model (InTEC) *Chen et al*., 2000] which integrates the effects of disturbance, climate, and atmospheric chemistry on the annual C cycle. These results can also contribute to future improvements in the Carbon budget model of the Canadian Forest Sector (CBM-CFS3) [*Kurz et al*., 2009] which is used in Canada's National Forest Carbon Monitoring, Accounting and Reporting System [*Stinson et al*., 2011] by replacing empirical yield functions with process-based representation of NPP and growth. This would improve the representation of the impacts of environmental drivers on the forest carbon balance. Moreover, such an approach would enable expanding estimates into the northern unmanaged forest areas for which inventory data and yield data are currently limited. The 250 m resolution reference NPP map could be used as a base for informing national-scale CBM-CFS3 simulation with InTEC results. In light of this, it is important that the NPP is mapped correctly; the distribution both at

watershed and regional scale is realistic; and the spatial distribution is resolved to the detailed maxima of spatial Fourier analysis over entire Canada, i.e., 200–300 m.

[42] The spatial distribution of our NPP map is relatively different from that reported by *Liu et al*. [2002]. The main reason is that our study reports NPP at 250 m spatial scale compared to 1 km used in *Liu et al*. [2002]; therefore, it captures extreme values better than the lumped 1 km simulations. It is the first time NPP is mapped at 250 m at daily timescale over Canada or for any other comparable region. The statistics are therefore potentially more accurate than previous results obtained for Canada at coarser spatial or temporal resolutions. The use of high resolution remotely sensed land cover, LAI, and clumping index maps made such simulation possible. The lack of significant systematic bias at annual level comparison of simulated and measured GPP gives us confidence in the Canada-wide NPP spatial distribution patterns and the regional statistics presented in this paper. *Liu et al*. [2002] reported the annual NPP for Canada's land area to be 1.27 Pg C for 1994 which is exactly the same as our estimates for 2008. However, there is strong spatial, land cover, ecozone differences between the *Liu et al*. [2002] and our NPP estimates. The *Liu et al*. [2002] NPP estimate does not include the contribution of understorey vegetation; the estimate from this study does. The differences of forest fire occurrences, harvests and insect-induced mortality, improvement in the model phenology and nutrient release schemes, and land cover maps between the *Liu et al*. [2002] and this study contribute to the differences between the NPP estimates from the two studies. Various studies have reported mean NPP of broadleaf deciduous forest to be between 315 and 781 g C $m^{-2} y^{-1}$, mixed forest 316 and 920 g C $m^{-2} y^{-1}$, and needleleaf forest 226 and 833 g C $m^{-2} y^{-1}$ [*Lieth and Robert*, 1975; *Melillo et al*., 1993; *Potter et al*., 1993; *Bonan*, 1995; *Prince et al*., 1995].

[43] A recent global NPP metaanalysis by *Ito* [2011] shows high uncertainty of NPP estimates in all methods (inventory, remote sensing, process models, and dynamic vegetation models) even for post-IBP estimates. Even the works published after year 2000 report global NPP to be between 37 and 83.8 Pg C y^{-1} [*Ito*, 2011]. Therefore, wide ranges of uncertainties remain in current estimates of NPP even using advanced biogeochemical and dynamic vegetation models and remote sensing techniques.

[44] Figures 4c and 4d present the statistics of BEPSd and BEPSh model structural errors, using simulations with site level LAI, meteorology, and V_m inputs. Both model simulations explain the measured GPP variability by more than 84%. The remaining unexplained variability can be attributed to the limitations of empirical stomatal conductance, soil inputs, and some of the unknown and missing model processes and equations, difference in flux footprint areas, indicating rooms for further improvement. We conclude that the NPP estimates presented in this study, despite different spatial distribution compared to the previous estimates, are more realistic. We have used improved LAI, clumping index, land cover, high resolution and optimized inputs, better phenology consideration, and improved BEPS model. The higher-resolution simulation enhances not only the characterization of input surface variables but also the parameterization of photosynthesis and respiration rates since at higher resolution, land cover types are less mixed.

[45] Due to computational constraints, we could not simulate hourly Canada-wide NPP at 250 m. There are several future research avenues that can improve NPP and GPP mapping using BEPS. Although BEPS is now a mature model and has shown strong performances in two NACP model intercomparison studies [*Schwalm et al*., 2010; *Schaefer et al*., 2012], there is still room for further improvement. Future work will include further diagnostic error assessments together with data assimilation and parameter optimization techniques. These results will then be compared with additional independent measurements obtained from forest inventory, tree ring analyses, and flux tower observations for various plant functional types.

[46] **Acknowledgments.** This study was supported by an NSERC Strategic grant (STPGP 381474–09). We thank the Fluxnet-Canada (Canadian Carbon Program) network; the site principal investigators, coinvestigators, participants, and data collection and processing staff for contributing to the tower flux data; and the agencies and institutions that funded long-term measurements at these sites. The 2005 North American Land Cover (NALC2005) at 250 m spatial resolution was produced by Natural Resources Canada/Canadian Centre for Remote Sensing (NRCan/CCRS), United States Geological Survey (USGS), Insituto Nacional de Estadística y Geografía (INEGI), Comisión Nacional para el Conocimiento y Uso de la Biodiversidad (CONABIO), and Comisión Nacional Forestal (CONAFOR).

References

Arain, A. A., and N. Restrepo-Coupe (2005), Net ecosystem production in a temperate pine plantation in southeastern Canada, *Agric. For. Meteorol.*, *128*, 223–241, doi:10.1016/j.agrformet.2004.10.003.

Arora, V. K., and G. J. Boer (2005), A parameterization of leaf phenology for the terrestrial ecosystem component of climate models, *Global Change Biol.*, *11*, 39–59, doi:10.1111/j.1365-2486.2004.00890.x.

Ball, J., L. E. Woodrow, and J. A. Beny (1987), A model predicting stomatal conductance and its contribution to the control of photosynthesis under different environmental conditions, in *Progress in Photosynthesis Research*, edited by J. Biggins, pp. 221–224, Martinus Nijhoff Publishers, Dordrecht, the Netherlands.

Barr, A. G., T. A. Black, E. H. Hogg, N. Kljun, K. Morgenstern, and Z. Nesic (2004), Inter-annual variability in the leaf area index of a boreal aspen-hazelnut forest in relation to net ecosystem production, *Agric. For. Meteorol.*, *126*, 237–255, doi:10.1016/j.agrformet.2004.06.011.

Barr, A. G., K. Morgenstern, T. A. Black, J. H. McCaughey, and Z. Nesic (2006), Surface energy balance closure by the eddy-covariance method above three boreal forest stands and implications for the measurement of the CO_2 flux, *Agric. For. Meteorol.*, *140*, 322–337, doi:10.1016/j.agrformet.2006.08.007.

Beerling, D. J., and W. P. Quick (1995), A new technique for estimating rates of carboxylation and electron-transport in leaves of C-3 plants for use in dynamic global vegetation models, *Global Change Biol.*, *1*, 289–294, doi:10.1111/j.1365-2486.1995.tb00027.x.

Bergeron, O., H. A. Margolis, T. A. Black, C. Coursolle, A. L. Dunn, A. G. Barr, and S. C. Wofsy (2007), Comparison of carbon dioxide fluxes over three boreal black spruce forests in Canada, *Global Change Biol.*, *13*, 89–107, doi:10.1111/j.1365-2486.2006.01281.x.

Bonan, G. B. (1995), Land atmosphere CO_2 exchange simulated by a land-surface process model coupled to an atmospheric general-circulation model, *J. Geophys. Res.*, *100*(D2), 2817–2831, doi:10.1029/94JD02961.

Bubier, J. L., R. Smith, S. Juutinen, T. R. Moore, R. Minocha, S. Long, and S. Minocha (2011), Effects of nutrient addition on leaf chemistry, morphology, and photosynthetic capacity of three bog shrubs, *Oecologia*, *167*, 355–368, doi:10.1007/s00442-011-1998-9.

Chen, B., J. M. Chen, G. Mo, C.-W. Yuen, H. Margolis, K. Higuchi, and D. Chan (2007), Modeling and scaling coupled energy, water, and carbon fluxes based on remote sensing: An application to Canada's landmass, *J. Hydrometeorol.*, *8*, 123–143, doi:10.1175/JHM566.1.

Chen, B., T. A. Black, N. C. Coops, T. Hilker, J. A. Trofymow, and K. Morgenstern (2009), Assessing tower flux footprint climatology and scaling between remotely sensed and eddy covariance measurements, *Boundary Layer Meteorol.*, *130*, 137–167, doi:10.1007/s10546-008-9339-1.

Chen, B., et al. (2011), Assessing eddy-covariance flux tower location bias across the Fluxnet-Canada Research Network based on remote sensing and footprint modelling, *Agric. For. Meteorol.*, *151*, 87–100, doi:10.1016/j.agrformet.2010.09.005.

Chen, J. M., and S. G. Leblanc (1997), A four-scale bidirectional reflectance model based on canopy architecture, *IEEE Trans. Geosci. Remote Sens.*, *35*, 1316–1337, doi:10.1109/36.628798.

Chen, J. M., J. Liu, J. Cihlar, and M. L. Goulden (1999), Daily canopy photosynthesis model through temporal and spatial scaling for remote sensing applications, *Ecol. Model.*, *124*, 99–119, doi:10.1016/S0304-3800(99)00156-8.

Chen, J. M., W. M. Ju, J. Cihlar, D. Price, J. Liu, W. J. Chen, J. J. Pan, A. Black, and A. Barr (2003), Spatial distribution of carbon sources and sinks in Canada's forests, *Tellus. B Chem. Phys. Meteorol.*, *55*, 622–641, doi:10.1034/j.1600-0889.2003.00036.x.

Chen, J. M., F. Deng, and M. Chen (2006a), Locally adjusted cubic-spline capping for reconstructing seasonal trajectories of a satellite-derived surface parameter, *IEEE Trans. Geosci. Remote Sens.*, *44*, 2230–2238, doi:10.1109/TGRS.2006.872089.

Chen, J. M., A. Govind, O. Sonnentag, Y. Zhang, A. Barr, and B. Amiro (2006b), Leaf area index measurements at Fluxnet-Canada forest sites, *Agric. For. Meteorol.*, *140*, 257–268, doi:10.1016/j.agrformet.2006.08.005.

Chen, J.M., G. Mo, J. Pisek, J. Liu, F. Deng, M. Ishizawa, and D. Chan (2012), Effects of foliage clumping on the estimation of global terrestrial gross primary productivity, *Global Biogeochem. Cycles*, *26*, GB1019, doi:10.1029/2010GB003996.

Chen, W. J., J. Chen, and J. Cihlar (2000), An integrated terrestrial ecosystem carbon-budget model based on changes in disturbance, climate, and atmospheric chemistry, *Ecol. Model.*, *135*, 55–79, doi:10.1016/S0304-3800(00)00371-9.

Contosta, A. R., S. D. Frey, and A. B. Cooper (2011), Seasonal dynamics of soil respiration and N mineralization in chronically warmed and fertilized soils, *Ecosphere*, *2*, 1–21, doi:10.1890/ES10-00133.1.

Coursolle, C., et al. (2006), Late-summer carbon fluxes from Canadian forests and peatlands along an east-west continental transect, *Can. J. For. Res.*, *36*, 783–800, doi:10.1139/x05-270.

Deng, F., J. M. Chen, S. Plummer, M. Chen, and J. Pisek (2006), Algorithm for global leaf area index retrieval using satellite imagery, *IEEE Trans. Geosci. Remote Sens.*, *44*, 2219–2229, doi:10.1109/TGRS.2006.872100.

Farquhar, G. D., S. V. Caemmerer, and J. A. Berry (1980), A biochemical-model of photosynthetic CO_2 assimilation in leaves of C-3 species, *Planta*, *149*, 78–90, doi:10.1007/BF00386231.

Gonsamo, A. (2011), Normalized sensitivity measures for leaf area index estimation using three-band spectral vegetation indices, *Int. J. Remote Sens.*, *32*, 2069–2080, doi:10.1080/01431161.2010.502153.

Gonsamo, A., and J. M. Chen (2011), Evaluation of the GLC2000 and NALC2005 land cover products for LAI retrieval over Canada, *Can. J. Remote Sens.*, *37*, 302–313, doi:10.5589/m11-039.

Gonsamo, A., and J. M. Chen (2013), Improved LAI algorithm implementation to MODIS data by incorporating background, topography and foliage clumping information, *IEEE Trans. Geosci. Remote Sens.*, doi:10.1109/TGRS.2013.2247405.

Gonsamo, A., J. M. Chen, C. Wu, and D. Dragoni (2012a), Predicting deciduous forest carbon uptake phenology by upscaling FLUXNET measurements using remote sensing data, *Agric. For. Meteorol.*, *165*, 127–135, doi:10.1016/j.agrformet.2012.06.006.

Gonsamo, A., J. M. Chen, D. T. Price, W. A. Kurz, and C. Wu (2012b), Land surface phenology from optical satellite measurement and CO_2 eddy covariance technique, *J. Geophys. Res.*, *117*, G03032, doi:10.1029/2012JG002070.

Groenendijk, M., et al. (2011), Seasonal variation of photosynthetic model parameters and leaf area index from global Fluxnet eddy covariance data, *J. Geophys. Res.*, *116*, G04027, doi:10.1029/2011JG001742

He, L., J. M. Chen, J. Pisek, C. B. Schaaf, and A. H. Strahler (2012), Global clumping index map derived from the MODIS BRDF product, *Remote Sens. Environ.*, *119*, 118–130, doi:10.1016/j.rse.2011.12.008.

Ito, A. (2011), A historical meta-analysis of global terrestrial net primary productivity: Are estimates converging?, *Global Change Biol.*, *17*, 3161–3175, doi:10.1111/j.1365-2486.2011.02450.x.

Jarvis, P. G. (1976), The interpretation of the variations in leaf water potential and stomatal conductance found in canopies in the field, *Philos. Trans. R. Soc. London B Biol. Sci.*, *273*, 593–610, doi:10.1098/rstb.1976.0035.

Jeffrey, S. J., J. O. Carter, K. B. Moodie, and A. R. Beswick (2001), Using spatial interpolation to construct a comprehensive archive of Australian climate data, *Environ. Modell. Software*, *16*, 309–330, doi:10.1016/S1364-8152(01)00008-1.

Ju, W., J. M. Chen, T. A. Black, A. G. Barr, J. Liu, and B. Chen (2006), Modelling multi-year coupled carbon and water fluxes in a boreal aspen forest, *Agric. For. Meteorol.*, *140*, 136–151, doi:10.1016/j.agrformet.2006.08.008.

Kurz, W. A., et al. (2009), CBM-CFS3: A model of carbon-dynamics in forestry and land-use change implementing IPCC standards, *Ecol. Model.*, *220*, 480–504, doi:10.1016/j.ecolmodel.2008.10.018.

Lafont, S., Y. Zhao, J. C. Calvet, P. Peylin, P. Ciais, F. Maignan, and M. Weiss (2012), Modelling LAI, surface water and carbon fluxes at high-resolution over France: Comparison of ISBA-A-gs and ORCHIDEE, *Biogeosciences*, *9*, 439–456, doi:10.5194/bg-9-439-2012.

Larjavaara, M., and H. C. Muller-Landau (2012), Temperature explains global variation in biomass among humid old-growth forests, *Global Ecol. Biogeogr.*, *21*, 998–1006, doi:10.1111/j.1466-8238.2011.00740.x.

Latifovic, R., Z. Zhu, J. Cihlar, C. Giri, and I. Olthof (2004), Land cover mapping of North and Central America—Global Land Cover 2000, *Remote Sens. Environ.*, *89*, 116–127, doi:10.1016/j.rse.2003.11.002.

Lieth, H., and H. W. Robert (1975), *Primary Productivity of the Biosphere*, Springer, New York.

Liu, J., J. M. Chen, J. Cihlar, and W. M. Park (1997), A process-based boreal ecosystem productivity simulator using remote sensing inputs, *Remote Sens. Environ.*, *62*, 158–175, doi:10.1016/S0034-4257(97)00089-8.

Liu, J., J. M. Chen, J. Cihlar, and W. Chen (1999), Net primary productivity distribution in the BOREAS region from a process model using satellite and surface data, *J. Geophys. Res.*, *104*(D22), 27,735–27,754, doi:10.1029/1999JD900768.

Liu, J., J. M. Chen, J. Cihlar, and W. Chen (2002), Net primary productivity mapped for Canada at 1-km resolution, *Global Ecol. Biogeogr.*, *11*, 115–129, doi:10.1046/j.1466-822X.2002.00278.x.

Melillo, J. M., A. D. McGuire, D. W. Kicklighter, B. Moore, C. J. Vorosmarty, and A. L. Schloss (1993), Global climate-change and terrestrial net primary production, *Nature*, *363*, 234–240, doi:10.1007/s10584-012-0460-2.

Middleton, E. M., J. H. Sullivan, B. D. Bovard, A. J. Deluca, S. S. Chan, and T. A. Cannon (1997), Seasonal variability in foliar characteristics and physiology for boreal forest species at the five Saskatchewan tower sites during the 1994 Boreal Ecosystem-Atmosphere Study, *J. Geophys. Res.*, *102*, 28,831–28,844, doi:10.1029/97JD02560.

Migliavacca, M., O. Sonnentag, T. F. Keenan, A. Cescatti, J. O'Keefe, and A. D. Richardson (2012), On the uncertainty of phenological responses to climate change, and implications for a terrestrial biosphere model, *Biogeosciences*, *9*, 2063–2083, doi:10.5194/bg-9-2063-2012.

Payeur-Poirier, J.-L., C. Coursolle, H. A. Margolis, and M.-A. Giasson (2012), CO_2 fluxes of a boreal black spruce chronosequence in eastern North America, *Agric. For. Meteorol.*, *153*, 94–105, doi:10.1016/j.agrformet.2011.07.009.

Pfeifer, M., M. Disney, T. Quaife, and R. Marchant (2012), Terrestrial ecosystems from space: A review of earth observation products for macroecology applications, *Global Ecol. Biogeogr.*, *21*, 603–624, doi:10.1111/j.1466-8238.2011.00712.x.

Pisek, J., and J. M. Chen (2009), Mapping forest background reflectivity over North America with Multi-angle Imaging SpectroRadiometer (MISR) data, *Remote Sens. Environ.*, *113*, 2412–2423, doi:10.1016/j.rse.2009.07.003.

Potter, C. S., J. T. Randerson, C. B. Field, P. A. Matson, P. M. Vitousek, H. A. Mooney, and S. A. Klooster (1993), Terrestrial ecosystem production: A process model based on global satellite and surface data, *Global Biogeochem. Cycles*, *7*, 811–841, doi:10.1029/93GB02725.

Prince, S. D., S. J. Goetz, and S. N. Goward (1995), Monitoring primary production from earth observing satellites, *Water Air Soil Pollut.*, *82*, 509–522, doi:10.1007/BF01182860.

Ren, W., H. Tian, B. Tao, A. Chappelka, G. Sun, C. Lu, M. Liu, G. Chen, and X. Xu (2011), Impacts of tropospheric ozone and climate change on net primary productivity and net carbon exchange of China's forest ecosystems, *Global Ecol. Biogeogr.*, *20*, 391–402, doi:10.1111/j.1466-8238.2010.00606.x.

Richardson, A. D., et al. (2011), Terrestrial biosphere models need better representation of vegetation phenology: Results from the North American Carbon Program Site Synthesis, *Global Change Biol.*, *18*, 566–584, doi:10.1111/j.1365-2486.2011.02562.x.

Running, S. W., and J. C. Coughlan (1988), A general model of forest ecosystem processes for regional applications I. Hydrologic balance, canopy gas-exchange and primary production processes, *Ecol. Model.*, *42*, 125–154, doi:10.1016/0304-3800(88)90112-3.

Santaren, D., P. Peylin, N. Viovy, and P. Ciais (2007), Optimizing a process-based ecosystem model with eddy-covariance flux measurements: A pine forest in southern France, *Global Biogeochem. Cycles*, *21*, GB2013, doi:10.1029/2006GB002834.

Schaefer, K., et al. (2012), A model-data comparison of gross primary productivity: Results from the North American Carbon Program site synthesis, *J. Geophys. Res.*, *117*, G03010, doi:10.1029/2012JG001960.

Schmidt, I. K., S. Jonasson, and A. Michelsen (1999), Mineralization and microbial immobilization of N and P in arctic soils in relation to season, temperature and nutrient amendment, *Appl. Soil Ecol.*, *11*, 147–160, doi:10.1016/S0929-1393(98)00147-4.

Schwalm, C. R., et al. (2010), A model-data intercomparison of CO_2 exchange across North America: Results from the North American Carbon Program site synthesis, *J. Geophys. Res.*, *115*, G00H05, doi:10.1029/2009JG001229.

Sellers, P. J., Y. Mintz, Y. C. Sud, and A. Dalcher (1986), A simple biosphere model (SiB) for use within general-circulation models,

J. Atmos. Sci., *43*, 505–531, doi:10.1175/1520-0469(1986)043<0505:ASBMFU>2.0.CO;2.

Sprintsin, M., J. M. Chen, A. Desai, and C. M. Gough (2012), Evaluation of leaf-to-canopy upscaling methodologies against carbon flux data in North America, *J. Geophys. Res.*, *117*, G01023, doi:10.1029/2010JG001407.

Stinson, G., W. A. Kurz, C. E. Smyth, E. T. Neilson, C. C. Dymond, J. M. Metsaranta, and D. Blain (2011), An inventory-based analysis of Canada's managed forest carbon dynamics, 1990 to 2008, *Global Change Biol.*, *17*, 2227–2244, doi:10.1111/j.1365-2486.2010.02369.x.

Trishchenko, A.P. (2004), The concept of new multiangular satellite mission for improved bi-directional sampling of surface and atmosphere properties, in *Proceedings of SPIE, the International Society for Optical Engineering*, pp. 97–108, SPIE, Bellingham, WA, doi:10.1117/12.560653.

Weiskittel, A. R., H. Temesgen, D. S. Wilson, and D. A. Maguire (2008), Sources of within- and between-stand variability in specific leaf area of three ecologically distinct conifer species, *Ann. For. Sci.*, *65*, 103–113, doi:10.1051/forest:2007075.

Wiken, E. B. (1986), Terrestrial ecozones of Canada, in Ecological Land Classification Series p. 26. Lands Directorate, Environment Canada.

Zhang, F., J. M. Chen, J. Chen, C. M. Gough, D. Dragoni, and T. A. Martin (2012), Evaluating spatial and temporal patterns of MODIS GPP over the conterminous U.S. against flux measurements and a process model, *Remote Sens. Environ.*, *124*, 717–729, doi:10.1016/j.rse.2012.06.023.

Zhao, M., and S. W. Running (2010), Drought-induced reduction in global terrestrial net primary production from 2000 through 2009, *Science*, *329*, 940–943, doi:10.1126/science.1192666.